Space-time characteristics of wall-pressure fluctuations in wall-modeled large eddy simulation

By G. I. Park AND P. Moin

1. Motivation and objectives

Pressure and shear stress fluctuations at the wall are of great importance in external hydro- and aerodynamics, since they are directly related to the structural vibration and noise generation from immersed bodies. Often the space-time characteristics of wall-pressure fluctuations are required for low-frequency sound propagation and vibration models.

In this brief, we focus on the prediction of fluctuating wall pressure and shear stress from wall-modeled large-eddy simulation (WMLES). WMLES is a technique to circumvent the prohibitive grid-resolution requirement in LES of high Reynolds number wall-bounded flows. In WMLES, the dynamically important but very small near-wall eddies are not directly resolved by the LES grid, but their effect is modeled by a wall model. In such an approach, one aims to compute the outer-layer using a coarse LES, while modeling the effect of momentum and heat transfer from the inner layer to the outer layer. Assessment of WMLES has always been based on the predictive quality of the mean velocity and Reynolds stresses. Secondary quantities from WMLES such as wall-pressure fluctuations and their spectra have received little attention, and are not reported. Here, the r.m.s. and wavenumber-frequency spectra of wall-pressure fluctuations are documented and analyzed. These supplementary data will elucidate to what extent the near-wall pressure field from WMLES can be utilized for modeling sound propagation and vibrations. A high Reynolds number turbulent channel flow is considered for this purpose.

2. Computational details

WMLES of a compressible channel flow is performed at $\mathrm{Re}_\tau = 2000$, the Reynolds number based on the channel half-height δ, the friction velocity u_τ, and the kinematic viscosity $\nu = \mu/\rho$. The Mach number at the channel centerline is fixed at 0.2 for comparison to the incompressible reference data. The size of the computational domain is $L_x = 25\delta$, $L_y = 2\delta$, and $L_z = 10\delta$ in the streamwise (x), wall-normal (y), and spanwise (z) directions, respectively. Incompressible DNS of Hoyas & Jiménez (2006) is used here as reference. In the baseline WMLES calculation, the grid spacings in wall units uniform in each direction are $(\Delta x^+,\ \Delta y^+,\ \Delta z^+) = (200,\ 40,\ 125)$. The number of grid points in the LES totals 4 million with $(N_x,\ N_y,\ N_z) = (250,\ 100,\ 160)$. In the fine WMLES calculation, the LES grid is refined only in the wall-parallel directions. Periodic boundary conditions are applied in the streamwise and spanwise directions, and the wall temperature is kept constant to balance the energy input from the source term by the wall-heat transfer. Since the coarse grid used in the LES cannot support the sharp velocity/temperature gradients at the wall, the usual no-slip/thermal wall-boundary conditions in the LES are replaced with approximate boundary conditions in terms of the wall stress/heat flux computed by the wall model. A non-equilibrium wall model which

solves unsteady 3-D Navier-Stokes equations on an embedded near-wall mesh with a RANS-type closure is used (see Park & Moin 2014; Park 2014 for details). The kinematic no-penetration condition is maintained. The non-equilibrium wall model was added to *Charles*, a cell-centered unstructured finite volume compressible LES solver provided by Cascade Technologies, Inc.

The space-time characteristics of wall-pressure fluctuations in the channel flow are analyzed in terms of wavenumber-frequency spectra, space/time two-point correlations, and convection velocity. The wavenumber spectra from WMLES are compared directly to the reference DNS data. The frequency spectrum of the DNS was obtained using the Taylor's hypothesis and the deduced convection velocity in the present study, because the DNS provides the power spectral density only in the wavenumber space. We follow the standard technique for computation of power spectra illustrated in Choi & Moin (1990). Pressure fluctuation signal at the wall $p(x, z, t)$ is collected over a non-dimensional time $T^+ = tu_\tau/\delta = 9.6$. The simulations time steps $\Delta t'$ are $1.25{\times}10^{-4}\delta/u_\tau$ and $1.0{\times}10^{-4}\delta/u_\tau$ for the coarse and the fine calculations, respectively. The sampling resolution is the same in both calculations, fixed at $\Delta t = 4{\times}10^{-3}\delta/u_\tau$. The signal is then divided into M overlapping intervals in the time domain with 50% overlap. Here we take $M = 12$. The Hanning window is applied to the signal within each interval to minimize spectral leakage in the frequency spectrum. Let $p^m(x, z, t)$ and $\hat{p}^m(k_1, k_3, \omega)$ be the pressure fluctuation signal in the m^{th} interval and its discrete Fourier transform. Here k_1, k_3, and ω are discrete wavenumbers and (angular) frequencies, which have both positive and negative components. First, the three-dimensional power spectral density $\phi(k_1, k_3, \omega)$ is calculated by

$$\phi(k_1, k_3, \omega) = \frac{1}{M} \sum_{m=1}^{M} |\hat{p}^m(k_1, k_3, \omega)|^2. \tag{2.1}$$

ϕ is then rescaled to satisfy the discrete Parseval's theorem,

$$\overline{p'^2} = \sum_{k_1, k_3, \omega} \phi(k_1, k_3, \omega). \tag{2.2}$$

In order to mimic an important property of the power spectrum in continuous space

$$\overline{p'^2} = \int_{-\infty}^{+\infty} E(k_1, k_3, \omega) dk_1 dk_3 d\omega, \tag{2.3}$$

the discrete three-dimensional power spectrum is defined as

$$\tilde{E}(k_1, k_3, \omega) = \frac{\phi(k_1, k_3, \omega)}{\Delta k_1 \Delta k_3 \Delta \omega}. \tag{2.4}$$

Two-dimensional power spectra are then obtained by integrating $\tilde{E}(k_1, k_3, \omega)$ over the remaining dimension

$$\tilde{E}(k_1, k_3) = \sum_{\omega} \tilde{E}(k_1, k_3, \omega)\Delta\omega, \quad \tilde{E}(k_1, \omega) = \sum_{k_3} \tilde{E}(k_1, k_3, \omega)\Delta k_3. \tag{2.5}$$

One-dimensional power spectra are obtained similarly

$$\tilde{E}(k_1) = \sum_{k_3, \omega} \tilde{E}(k_1, k_3, \omega)\Delta\omega\Delta k_3, \quad \tilde{E}(\omega) = \sum_{k_1, k_3} \tilde{E}(k_1, k_3, \omega)\Delta k_1 \Delta k_3. \tag{2.6}$$

Two-dimensional two-point auto-correlations $R(r_x, r_z)$ and $R(r_x, r_t)$ are calculated by

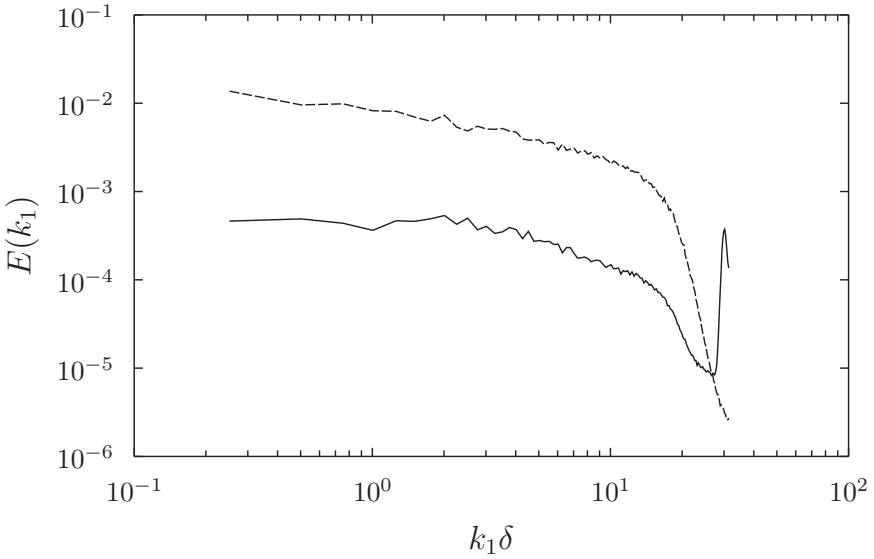

FIGURE 1. Power spectra of pressure (solid line) and streamwise velocity (dashed line) fluctuations from the present $\mathrm{Re}_\tau = 2003$ WMLES (baseline mesh). Each spectrum is normalized such that the total energy is equal to 1.

taking the inverse Fourier transform of the corresponding two-dimensional power spectra $\tilde{E}(k_1, k_3)$ and $\tilde{E}(k_1, \omega)$, and normalizing them with their respective maxima at zero separation. The one-dimensional spectra are often presented in the space of positive wavenumbers/frequencies, since they are symmetric about the zero wavenumber/frequency axes. For this purpose, single-sided one-dimensional spectra are defined by

$$E(k_1) = 2\tilde{E}(k_1), \quad E(k_3) = 2\tilde{E}(k_3), \quad E(\omega) = 2\tilde{E}(\omega). \tag{2.7}$$

3. Results

3.1. *R.m.s. fluctuation of wall pressure and shear stress*

Before presenting the results and comparing them to the incompressible DNS data, a few remarks are in order regarding an unexpected pressure behavior in the present compressible channel flow calculations. Strong 2-Δ waves in the streamwise direction were found from the pressure and density signals in the channel calculation (they were not present in the velocity fields, see Figure 1). The 2-Δ waves were also present in calculations without using a wall model (no-slip wall). These waves manifested themselves in the pile-up of energy at high wavenumbers ($0.91 \leq k_1/k_1^{max} \leq 1$, where k_1 is the streamwise wavenumber), possessing the highest energy and accounting for 19% of the total energy. The length scale associated with this energy pile-up was between $2\Delta x$ and $2.2\Delta x$. The spurious waves were not found in the initially laminar state, but they emerged through transition to turbulence and were trapped within the periodic channel. The amplitudes of the waves were highest at the wall and lowest near the channel centerline. The 2-Δ wave did not appear in the boundary layer and airfoil calculations presented in Park & Moin (2014), which had inlets and outlets. All these observations suggest that the 2-Δ wave is likely induced by poorly resolved acoustic waves trapped in the doubly periodic domain. Presumably, once generated, it persists for a long time owing to stiff flow con-

Case	$\Delta x^+/\Delta z^+$	$p'^+_{w,rms}$	$\tau'^+_{w,rms}$
Present WMLES (baseline)	200/125	3.98(3.22)	0.24
Present WMLES (xz-refined)	100/62.5	3.05(2.90)	0.25
Incomp. DNS (Hoyas & Jiménez 2006)	8.2/4.1	2.82	0.43

TABLE 1. Fluctuating wall pressure and shear stress in $\mathrm{Re}_\tau = 2003$ turbulent channel flow. Numbers in parentheses are $p'^+_{w,rms}$ obtained by excluding the 2-Δ wave contributions. $\tau'_w = \partial u'/\partial y$ is the wall-normal gradient of the streamwise velocity fluctuation at the wall.

ditions (high Reynolds number and low Mach number) and conservative/non-dissipative schemes used for nonlinear advection terms. Some dissipative *ad hoc* remedies, such as filtering the pressure signal every 10 time steps and adding 0.2% upwinding, helped reduce the amplitude of the 2-Δ wave, but they were not pursued owing to their negative effects on the mean flow.

The problem was mitigated when the baseline channel mesh was refined in the wall-parallel directions (x and z). The pile-up of energy still occurred in the range of $0.92 \leq k_1/k_1^{max} \leq 1$, but it possessed significantly lower energy than that in the coarse calculation, and accounted for only 5% of the total energy. In fact, it is shown in the subsequent section that, in the baseline mesh, the pressure fluctuations producing eddies were resolved with less than 2 and 5 cells in the streamwise and spanwise directions, respectively. Further mesh refinement to remove the energy pile-up at high wavenumbers was not performed, since it would approach the limit of resolved LES which does not require the wall model.

Table 1 shows the fluctuating wall pressure and shear stress ($p'^+_{w,rms}$ and $\tau'^+_{w,rms}$) from the turbulent channel flow. Note that the current wall model does not model the wall pressure, and provides only the wall-shear stress to the LES. Therefore, $\tau'^+_{w,rms}$ is calculated from the wall model solution, whereas $p'^+_{w,rms}$ comes from the LES solution. $p'^+_{w,rms}$ in the channel flow is overpredicted by a factor of 1.4 with the baseline mesh, and by a factor of 1.08 with the LES mesh refined in the wall-parallel directions. However, when the contribution from the 2-Δ wave is excluded, $p'^+_{w,rms}$ is overpredicted only by a factor of 1.14 and 1.03 with the baseline and refined meshes, respectively. It is anticipated that, with finer grids, $p'^+_{w,rms}$ will eventually converge to the DNS value and the spurious wave will be suppressed.

On the contrary, $\tau'^+_{w,rms}$ is insensitive to the LES mesh resolution and remains to be significantly underpredicted ($\sim$50% of the DNS value). It is suspected that the wall model, with a highly diffusive RANS-type turbulence parameterization and an upwinding advection scheme, damps out the footprint of fluctuating LES signals imposed on the top boundary. In fact, a RANS based wall model is responsible only for producing the correct mean wall-shear stress. Therefore, the resolved fluctuation of the wall-shear stress is not represented adequately in the wall model, and it is insensitive to the mesh refinement in the outer layer.

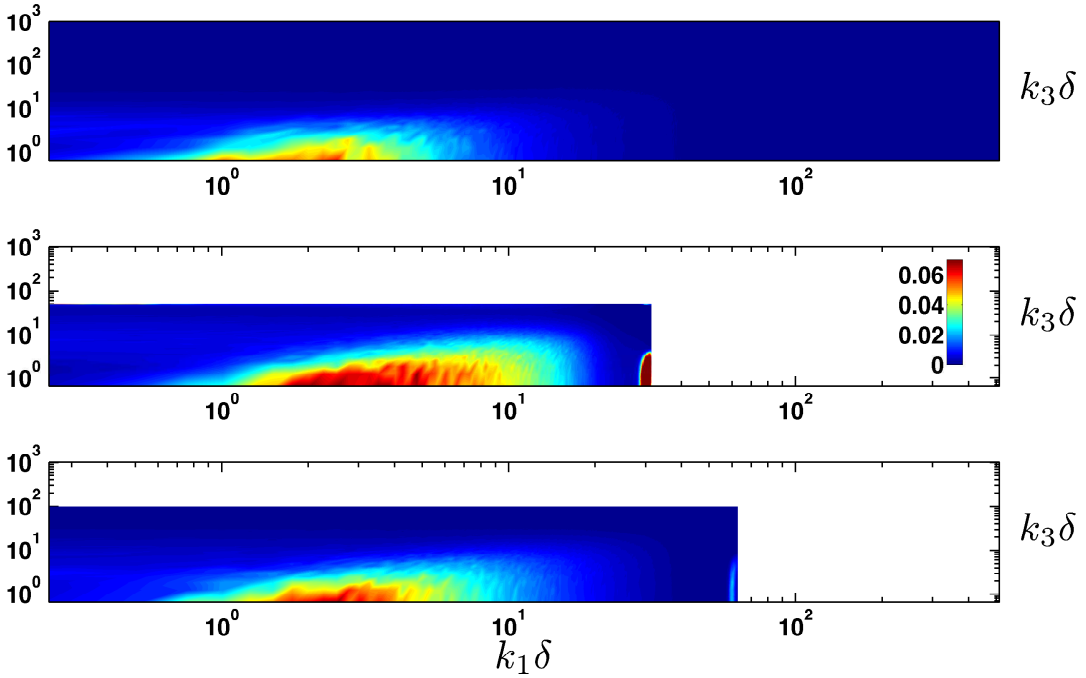

FIGURE 2. Contour plot of two-dimensional streamwise/spanwise wavenumber power spectrum of wall-pressure fluctuations ($E(k_1, k_3)/\tau_w^2\delta^2$) . Top, DNS of Hoyas & Jiménez (2006); middle, present WMLES (baseline mesh); bottom, present WMLES (xz-refined mesh).

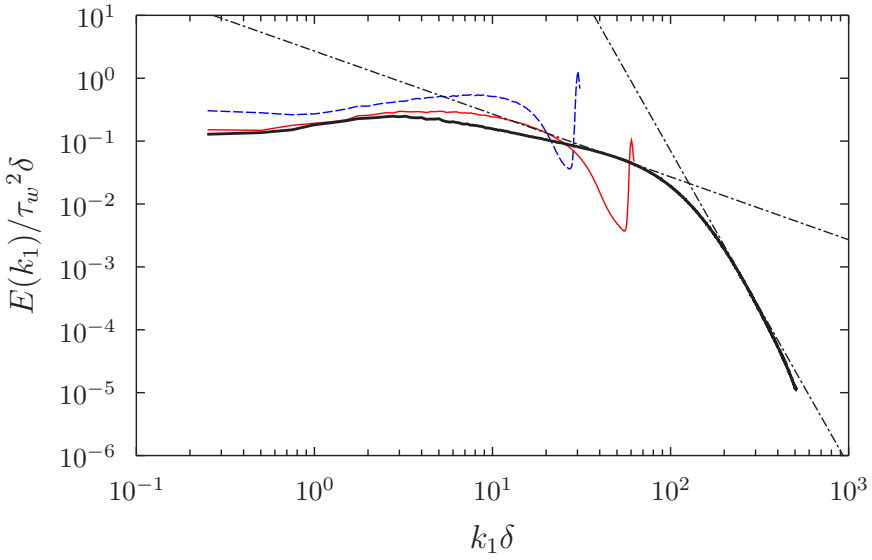

FIGURE 3. Streamwise wavenumber spectrum of wall-pressure fluctuations. Blue dashed line, present WMLES (baseline mesh); red solid line, present WMLES (xz-refined mesh); black solid line (with the longest tail), DNS of Hoyas & Jiménez (2006); dashed-dotted lines, -1 and -5 slope lines.

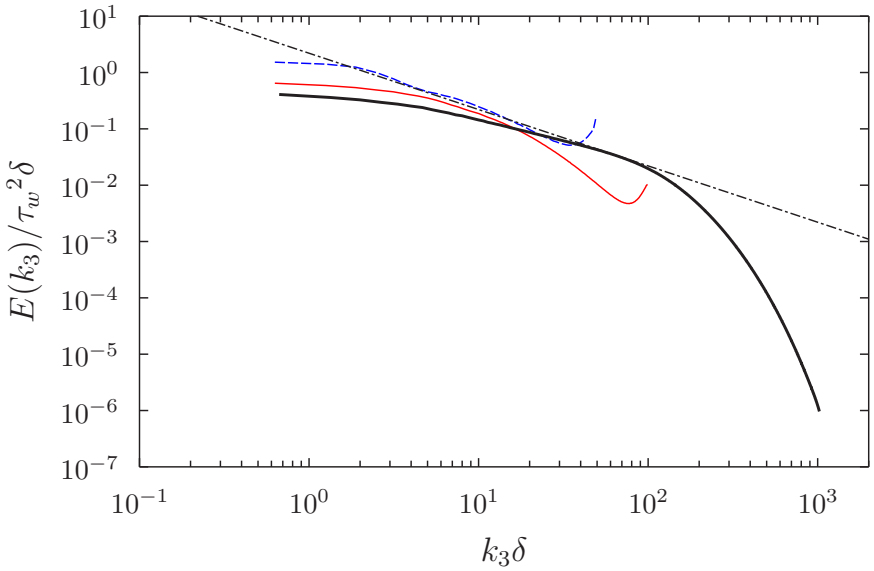

FIGURE 4. Spanwise wavenumber spectrum of wall-pressure fluctuations. Blue dashed line, present WMLES (baseline mesh); red solid line, present WMLES (xz-refined mesh); black solid line (with the longest tail), DNS of Hoyas & Jiménez (2006); dashed-dotted line, -1 slope.

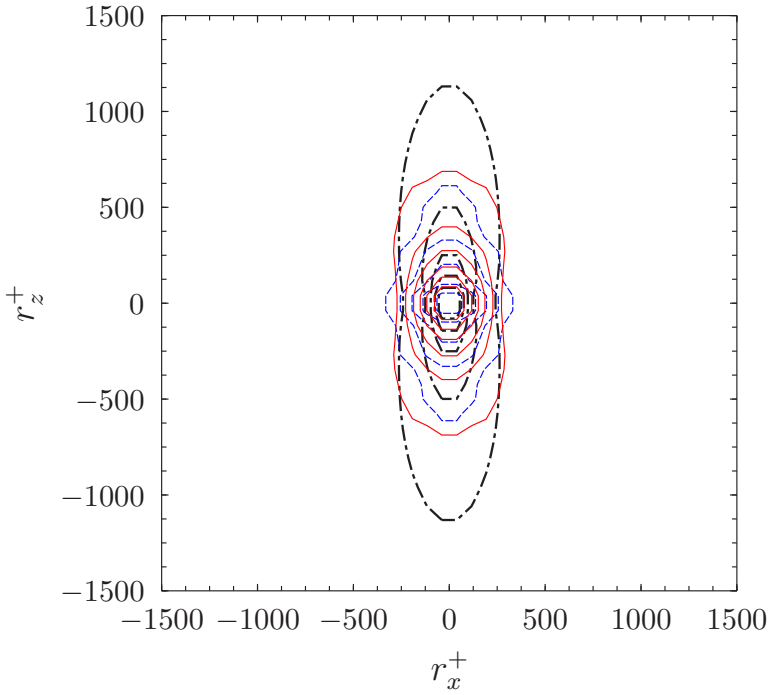

FIGURE 5. Contours of two-point auto-correlation of wall-pressure fluctuations $R(r_x, r_z)$ as a function of streamwise and spanwise separations. Contour levels from 0.1 with 0.1 increment. Blue dashed line, present WMLES (baseline mesh); red solid line, present WMLES (xz-refined mesh). black dash-dotted line, DNS of Hoyas & Jiménez (2006) reported in Sillero *et al.* (2014).

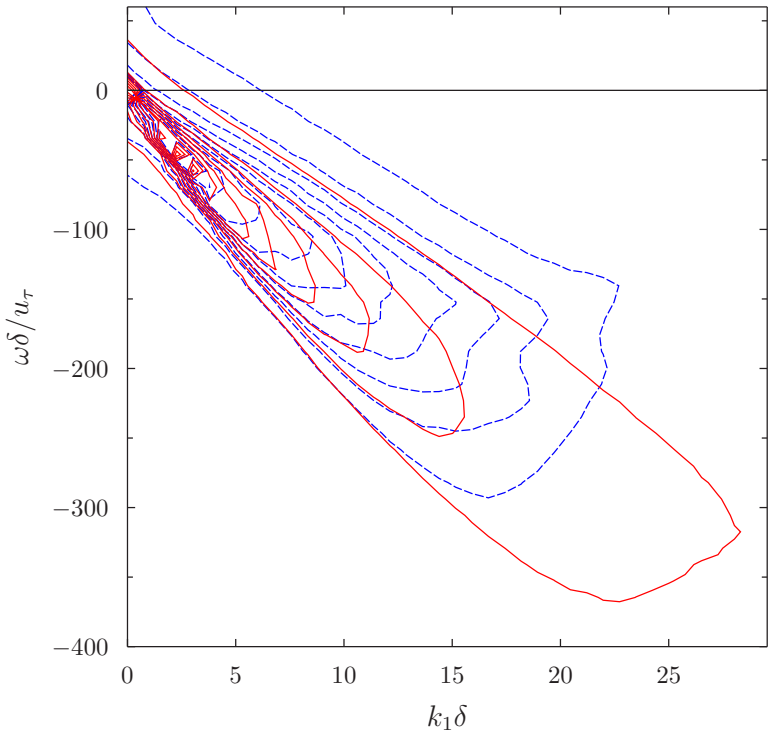

FIGURE 6. Contours of two-dimensional streamwise wavenumber-frequency power spectrum of wall-pressure fluctuations ($E(k_1,\omega)u_\tau/\tau_w^2\delta^2$). Contour levels from 0.002 to 0.004 with 0.0002 increment. Blue dashed line, present WMLES (baseline mesh); red solid line, present WMLES (xz-refined mesh).

3.2. *Space-time characteristics of wall-pressure fluctuations*

Figure 2 shows the contour plots of the streamwise/spanwise wavenumber spectrum $E(k_1,k_3)$. In the coarse WMLES, a high energy density associated with the 2-Δ wave is visible in the lower right corner. Since the one-dimensional spectra are obtained by reducing (summing) $E(k_1,k_3)$ in the remaining direction, it is evident that the 2-Δ wave contaminates $E(k_1)$ in high k_1 and $E(k_3)$ in low k_3. This is reflected in the plots of $E(k_1)$ and $E(k_3)$ shown below. Additionally, the total energy ($\overline{p'^2}$) is overpredicted, and the energy distribution is biased towards the high wavenumber region compared to the incompressible DNS. In the fine WMLES, the influence of the 2-Δ wave is much weaker and a better agreement with the DNS is observed.

Figure 3 shows the streamwise wavenumber spectrum $E(k_1)$. The 2-Δ wave is clearly visible in both the coarse and fine calculations, while it is less severe in the latter. As mentioned earlier, 19% (coarse mesh) and 5% (fine mesh) of the total (pressure) energy are contained in the rising tails of the spectra. Note that the low-wavenumber spectrum from the fine calculation is in good agreement with the reference DNS. A -1 slope and a -5 slope in the spectrum are known to be related to turbulence in the logarithmic layer and the buffer layer, respectively (Bradshaw 1967). The power spectra from both WMLES and DNS exhibit a short -1 slope region, and a relatively well-developed -5 slope in the high-wavenumber region. Figure 4 shows the spanwise wavenumber spectrum $E(k_3)$.

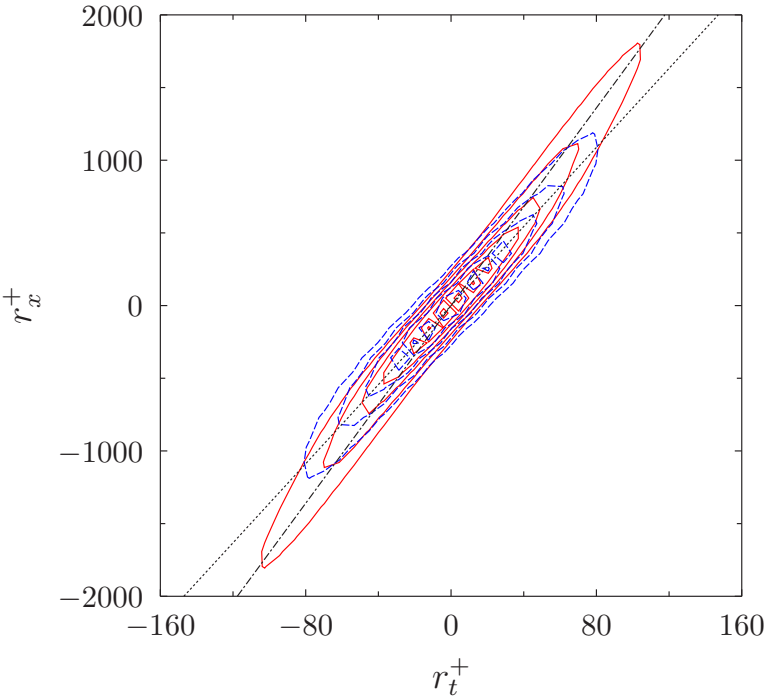

FIGURE 7. Contours of two-point auto-correlation of wall-pressure fluctuations $R(r_x, r_t)$ as a function of streamwise and temporal separations. Contour levels from 0.2 to 0.9 with 0.1 increment. Blue dashed line, present WMLES (baseline mesh); red solid line, present WMLES (xz-refined mesh); black dashed line, denotes $U_c = 13.6u_\tau = 0.56U_0$; black dashed-dotted line, denotes $U_c = 17u_\tau = 0.7U_0$; $u_\tau = \sqrt{\tau_w/\rho}$ is the friction velocity, and U_0 is the channel center-line velocity.

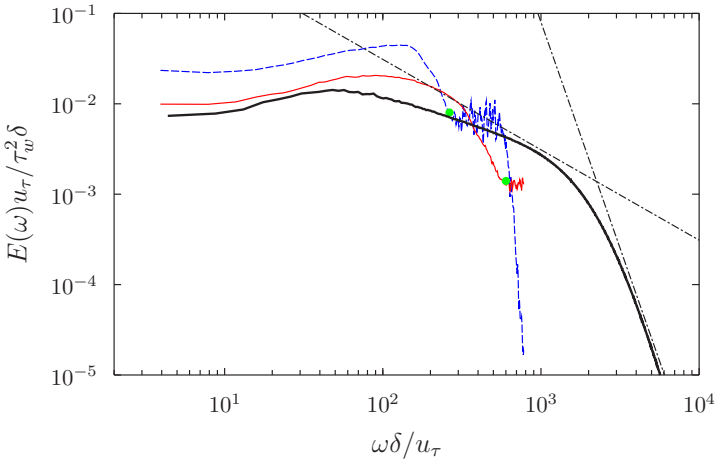

FIGURE 8. Frequency spectrum of wall-pressure fluctuations. Blue dashed line, present WMLES (baseline mesh); red solid line, present WMLES (xz-refined mesh); black solid line (with the longest tail), DNS of Hoyas & Jiménez (2006). We deduced the frequency spectrum of the DNS from $E(k_1)^{DNS}$ using the Taylor's hypothesis with $U_c = 0.7U_0$; dashed-dotted lines, -1 and -5 slope lines; green circles; cut-off frequency ω_c based on the streamwise grid spacing ($4\Delta x$) in WMLES and the convection velocity $0.7U_0$.

The spectrum from the fine calculation is in better agreement with the DNS in the low-wavenumber region.

Figure 5 shows the two-point spatial auto-correlation of wall-pressure fluctuations as a function of streamwise and spanwise separations. It can be deduced that the integral length scales of the pressure-producing near-wall eddies are about 250 and 1000 wall units in the streamwise and spanwise directions, respectively. In the outer layer scaling, they are 0.125δ and 0.5δ in the streamwise and spanwise directions, respectively. Obviously, these eddies are not resolved at all in the coarse WMLES, and they are resolved marginally in the fine WMLES (see Table 1). The contours in the DNS and the fine WMLES have circular shapes at small separations and oval shapes elongated in the spanwise direction at large separations. This is consistent with the findings from previous studies (Willmarth 1975; Choi & Moin 1990).

Figures 6 and 7 show the contours of the two-dimensional streamwise wavenumber-frequency power spectrum $E(k_1, \omega)$, and the contours of the two-point auto-correlation $R(r_x, r_t)$. The strong convective nature of wall-pressure fluctuations is reflected on the contours clustered in a thin band. The slope of this narrow band is interpreted as the convection velocity U_c of wall-pressure fluctuations. While it is possible to obtain U_c as a function of k_1 and ω, we define U_c simply to be the slope of the best line fit to the contours of $R(r_x, r_t)$ in the range of [0.3, 0.9]. The convection velocities obtained in this manner are U_c=$0.56U_0$ and U_c=$0.7U_0$ in the coarse and the fine calculations, respectively, where U_0 is the channel centerline velocity. U_c in the finer calculation is in good agreement with the overall convection velocity of the most energetic structures in low Reynolds number channel flows reported by Kim (1989), Choi & Moin (1990), and Jeon *et al.* (1999) ($U_c \approx 0.72U_0$).

Lastly, Figure 8 shows the frequency power spectrum $E(\omega)$. Both the coarse and the fine calculations exhibit wiggles in the spectra in the frequency range of $\omega > \omega_c$, where $\omega_c = \pi U_c/4\Delta x$ is the frequency of a streamwise wave with a 4-Δx wavelength, convected with velocity U_c=$0.7U_0$. The effect of the spurious 2-Δx wave described earlier is dominant in this frequency range, and the frequency spectrum is contaminated. Note that the wiggles are much weaker in the fine calculation. In this figure, the frequency spectrum of the DNS that is deduced from $E(k_1)^{DNS}$ is also plotted. Using Taylor's frozen turbulence hypothesis, a streamwise wave with a wavenumber k_1 is assumed to be convected with the convection velocity U_c. The dispersion relation is then given as $\omega = k_1 U_c$, from which the frequency spectrum can be deduced as

$$\overline{p'^2} = \int_0^\infty E(k_1)^{DNS} dk_1 = \int_0^\infty \frac{E(\omega/U_c)^{DNS}}{U_c} d\omega. \tag{3.1}$$

The integrand of the last term in the above equation is the frequency spectrum deduced using the Taylor's hypothesis. Here we take $U_c = 0.7U_0$ from the fine WMLES calculation. The spectrum from the fine WMLES calculation in the low-frequency band is in a reasonable agreement with the deduced DNS spectrum. Both the fine WMLES and the DNS have a short -1 slope region, and a relatively well-developed -5 slope high-frequency region.

4. Conclusion

In summary, the space-time characteristics of wall-pressure fluctuations obtained from WMLES of a channel flow agree reasonably well with the DNS data, provided that the

pressure-producing structures are resolved by the LES grid. Based on comparison of spatial spectra with DNS, it appears that at least 4 cells per integral length scale are required in the streamwise direction, and about 10 cells per integral length scale in the spanwise direction. This corresponds to $\delta/\Delta x \geq 20$ and $\delta/\Delta z \geq 32$ in terms of the grid spacings in the outer scaling. Otherwise the pressure statistics are overpredicted, and can potentially be contaminated by the spurious 2-Δ waves. When these conditions were met, the spectra in the low-wavenumber/low-frequency region were predicted reasonably well. However, wall-stress fluctuations modeled entirely through a RANS-based wall model are largely underpredicted and insensitive to the LES grid refinement. Based on this observation, we suspect that pressure fluctuations in wall-bounded flows are mostly outer-layer phenomena and therefore their prediction improves with the grid refinement in outer-layer scales. On the other hand, proper representation of short-time scale, small near-wall eddies seems to be important for correct prediction of wall shear stress fluctuations, and hence the present RANS-based wall model does not predict them accurately.

Acknowledgments

This work was supported jointly by NASA Aeronautics Scholarship Program, NASA under the Subsonic Fixed-Wing Program (Grant No. NNX11AI60A), and the Boeing Company. Computations were carried out on the US DOE advanced computational facilities at Los Alamos National Laboratory and Lawrence Livermore National Laboratory. The authors are grateful to Professor Jiménez and Dr. Sillero for providing the raw DNS data (the wavenumber spectra and spatial two-point correlation).

REFERENCES

Bradshaw, P. 1967 Inactive motion and pressure fluctuations in turbulent boundary layers. *J. Fluid Mech.* **30**, 241–258.

Choi, H. & Moin, P. 1990 On the space-time characteristics of wall-pressure fluctuations. *Phys. Fluids* **2**, 1450–1460.

Hoyas, S. & Jiménez, J. 2006 Scaling of the velocity fluctuations in turbulent channels up to $Re_\tau = 2003$. *Phys. Fluids* **18**, 011702.

Jeon, S., Choi, H., Yoo, J. & Moin, P. 1999 Space-time characteristics of the wall shear-stress fluctuation in a low Reynolds number channel flow. *Phys. Fluids* **11**, 3084–3094.

Kim, J. 1989 On the structure of pressure fluctuations in simulated turbulent channel flow. *J. Fluid Mech.* **205**, 421–451.

Park, G. I. 2014 *Wall-modeled large eddy simulation in an unstructured mesh environment.* Ph.D Thesis, Stanford University.

Park, G. I. & Moin, P. 2014 An improved dynamic non-equilibrium wall-model for large eddy simulation. *Phys. Fluids* **26**, 015108.

Sillero, J. A., Jiménez, J. & Moser, R. D. 2014 Two-point statistics for turbulent boundary layers and channels at Reynolds numbers up to $\delta^+ \approx 2000$. *Phys. Fluids* **26**, 105109.

Willmarth, W. W. 1975 Pressure fluctuations beneath turbulent boundary layers. *Annu. Rev. Fluid Mech.* **7**, 13–36.